A Sliding-Mode Direct Power Control Strategy for DFIG Under Both Balanced and Unbalanced Grid Conditions Using Extended Active Power

Dan Sun, *Member, IEEE*, Xiaohe Wang, Heng Nian, *Senior Member, IEEE*, and Z. Q. Zhu, *Fellow, IEEE*

***Abstract*—This paper proposes a sliding-mode direct power control (SMDPC) strategy for doubly fed induction generator (DFIG) under both balanced and unbalanced grid conditions using extended active power. When the traditional power theory is used under unbalanced grid condition, the control strategies usually need to be modified and become more complicated. Therefore, an extended active power is proposed in this paper, which is effective under both balanced and unbalanced grid conditions with a simple control strategy. Based on the extended active power, elaborated analysis of the mathematical model of DFIG is obtained. Furthermore, an SMDPC strategy using the extended active power is proposed, which can obtain sinusoidal stator currents and restrain electromagnetic torque ripples under unbalanced grid condition without the need of decomposition process and phase-locked loop (PLL). Comparative experimental studies of the SMDPC using the extended and traditional active powers for DFIG are conducted to validate the effectiveness of the proposed strategy under both balanced and unbalanced grid conditions. In addition, the dynamic performance and robustness of the proposed SMDPC are also proved to be satisfying by the experimental results.**

***Index Terms*—Doubly fed induction generator (DFIG), extended active power, sliding-mode control (SMC), unbalanced grid condition.**

NOMENCLATURE

$\boldsymbol{\psi_s}$, $\boldsymbol{\psi_r}$	Stator, rotor flux linkage phasors.
$\boldsymbol{U_s}$, $\boldsymbol{U_r}$	Stator, rotor voltage phasors.
$\boldsymbol{I_s}$, $\boldsymbol{I_r}$	Stator, rotor current phasors.
P_s, Q_s	Stator output active, reactive powers.
R_s, R_r	Stator, rotor resistances.
L_s, L_r, L_m	Stator, rotor self-inductances and mutual inductance.
L_{ls}, L_{lr}	Stator, rotor leakage inductances.
ω_1, ω_r, ω_{slip}	Synchronous, rotor and slip angular frequencies.

Manuscript received October 4, 2016; revised December 31, 2016; accepted March 20, 2017. Date of publication March 23, 2017; date of current version November 2, 2017. This work was supported by the National Natural Science Foundation of China under Grants 51377141 and 51622706. Recommended for publication by Associate Editor S. Williamson. *(Corresponding author: Dan Sun.)*

D. Sun, X. Wang, and H. Nian are with the College of Electrical Engineering, Zhejiang University, Hangzhou 310027, China (e-mail: sundan@zju.edu.cn; 21410053@zju.edu.cn; nianheng@zju.edu.cn).

Z. Q. Zhu is with the Department of Electronic and Electrical Engineering, University of Sheffield, Sheffield, S1 3JD, U.K. (e-mail: z.q.zhu@sheffield.ac.uk).

Color versions of one or more of the figures in this paper are available online at http://ieeexplore.ieee.org.

Digital Object Identifier 10.1109/TPEL.2017.2686980

I. INTRODUCTION

THANKS to the attractive features of variable-speed operation, four-quadrant running capability, and lower power loss compared with other solutions, doubly fed induction generator (DFIG) has become the most popular form in present wind power generation systems [1], [2]. The mainstream control strategies for DFIG are vector control (VC) and direct power control (DPC). VC can achieve excellent steady-state performance by decomposing the currents into active and reactive components and regulate them separately using PI controllers. However, it cannot guarantee a satisfying dynamic performance because of the lag effect of integrators. In addition, the control system is complicated and the phase-locked loop (PLL) is needed to change the system into synchronous reference frame [3], [4]. Therefore, DPC has been proposed as an alternative approach. Traditional lookup-table-based direct power control (LUT-DPC) shows advantages of fast dynamic response and simple structure. However, large power ripples exist because of the hysteresis comparator, and the switching frequency is variable [5], [6].

As an effective nonlinear control strategy, the sliding-mode control (SMC) strategy has received much attention [7]–[10]. In [7], the SMC strategy is first applied to electrical drive systems. Due to the features of disturbance rejection and simple implementation, it shows great perspective in industrial applications. Further studies combine SMC techniques with the DPC strategies, and a sliding-mode direct power control (SMDPC) strategy is proposed for the power converter [8], [9]. The fast dynamic response is inherited from the traditional LUT-DPC, and the steady-state performance is also satisfying. In addition, the robustness of the control system is pretty good. Hu *et al*. [10] propose an SMDPC strategy for DFIG, and the effectiveness is verified by simulation results. However, the control strategies analyzed earlier are all based on balanced grid condition. Because of the direct connection between the DFIG stator and the grid, the DFIG system is quite sensitive to grid disturbances [11]–[23]. Therefore, the DFIG might be disconnected from the network to protect themselves under unbalanced grid condition, which is not allowed by the modern grid codes [11].

Various control strategies are proposed for DFIG under unbalanced grid condition. In [12] and [13], two sets of PI controllers are used to control the positive and negative current components, respectively. It can achieve a good steady-state performance. However, the positive and negative components decomposition significantly increases the computational burdens of the control system. Resonant controllers have been widely used in the control strategy under unbalanced grid condition due to the control effect on the variables of specific frequency. Current control strategies based on a proportional–resonant (PR) controller and a proportional–integral–resonant (PIR) controller are proposed in [14] and [15], respectively. Different control targets can be achieved by giving different reference values of positive and negative sequence current components. The experimental results indicate that both can work well under unbalanced grid condition. However, the current reference is still calculated based on the decomposition process.

Power compensation strategy is proposed as an improved method for DPC under unbalanced grid condition, which can achieve various control targets by adding different compensations to the reference power [16], [17]. However, the positive and negative components are still needed to calculate the compensation power. A PI-based control strategy with a resonant compensator is proposed in [18] and [19]. The specific control targets are used as the reference values for the resonant compensator rather than the negative sequence current components. Thus, the decomposition process can be eliminated. However, the control system is based on the synchronous reference frame and the rotating coordinate transformation is still needed, which will also increase the computational burdens. In addition, the control performance depends on the parameter turning of the PI controller and resonant controller.

The control strategies analyzed earlier are all based on the traditional power theory. The control system is complicated, and the decomposition process and rotating coordinate transformation significantly increase the computational burdens, which require a higher CPU capability. An extended reactive power is proposed for ac/dc converter in [20]. The control system is based on the frame of VC and the current reference calculation still requires the positive and negative components of grid voltages and currents. In order to avoid this disadvantage, the extended reactive power is combined with DPC strategies and applied to the ac/dc converter under unbalanced grid condition [21]–[23]. Experimental results verify that the strategies can restrain the active power ripples and obtain sinusoidal stator currents without the need of decomposition process. However, using the extended reactive power cannot restrain the electromagnetic torque ripples for DFIG under unbalanced grid condition, which is very harmful to wind turbine systems.

The main contribution of this paper is to propose an SMDPC strategy for DFIG using extended active power, which can obtain sinusoidal stator currents and restrain electromagnetic torque ripples under unbalanced grid condition without the need of decomposition process and PLL block. Therefore, the control system is simple and the computational burdens of CPU can be reduced. The rest of this paper is organized as follows. In Section II, the extended active power is proposed and the new control target is selected based on the analysis of power components. In addition, an elaborated analysis of the mathematical model of DFIG is made based on the extended active power to obtain the proper formulae for SMDPC strategy. Then, in Section III, the SMDPC using extended active power is applied to DFIG. Comparative experimental studies of the SMDPC using the extended and traditional active powers are conducted to confirm the effectiveness of the proposed strategy under both balanced and unbalanced grid conditions in Section IV. Finally, the conclusion is made in Section V.

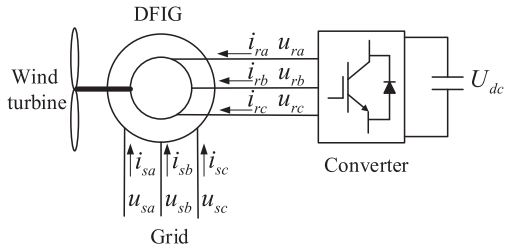

Fig. 1. Topology of the DFIG for wind power generation.

II. Model of DFIG Under Unbalanced Grid Condition Using Extended Active Power

Topology of the DFIG for wind power generation is illustrated in Fig. 1, where $i_{\rm sa}$, $i_{\rm sb}$, and $i_{\rm sc}$ are the stator currents; $u_{\rm sa}$, $u_{\rm sb}$, and $u_{\rm sc}$ are the stator voltages; $i_{\rm ra}$, $i_{\rm rb}$, and $i_{\rm rc}$ are the rotor currents; $u_{\rm ra}$, $u_{\rm rb}$, and $u_{\rm rc}$ are the rotor voltages; and $U_{\rm dc}$ is the dc-bus voltage. The direction of the voltage is in consistent with the current.

The traditional power can be expressed as

$$\begin{cases} P_s = \dfrac{3}{2}\mathrm{Re}(\boldsymbol{I}^*_{s\alpha\beta}\boldsymbol{U}_{s\alpha\beta}) \\ Q_s = \dfrac{3}{2}\mathrm{Im}(\boldsymbol{I}^*_{s\alpha\beta}\boldsymbol{U}_{s\alpha\beta}) \end{cases} \tag{1}$$

where "$*$" denotes the conjugate of complex phasors.

When the traditional power is selected as the control target under unbalanced grid condition, there will be third sequence harmonic components in stator currents, and the electromagnetic torque will contain oscillating components at twice the grid frequency, which is very harmful to the power grid as well as the generator itself [17]. Therefore, the control strategy needs to be more complicated when the traditional power is used under unbalanced grid condition.

An extended active power is proposed in this paper, which can be expressed as

$$P_s^{\rm new} = -\frac{3}{2}\mathrm{Im}(\boldsymbol{I}^*_{s\alpha\beta}\boldsymbol{U}'_{s\alpha\beta}) \tag{2}$$

where $U'_{s\alpha\beta}$ lags $U_{s\alpha\beta}$ by a quarter of the fundamental period.

Under unbalanced grid condition, the positive and negative sequence components of voltage and current in the stationary

reference frame can be expressed as

$$\begin{cases} u_{s\alpha+} = |\boldsymbol{U}_{s+}|\cos(\omega_1 t + \theta_{u+}), \\ u_{s\beta+} = |\boldsymbol{U}_{s+}|\sin(\omega_1 t + \theta_{u+}) \\ u_{s\alpha-} = |\boldsymbol{U}_{s-}|\cos(-\omega_1 t + \theta_{u-}), \\ u_{s\beta-} = |\boldsymbol{U}_{s-}|\sin(-\omega_1 t + \theta_{u-}) \end{cases} \tag{3}$$

$$\begin{cases} i_{s\alpha+} = |\boldsymbol{I}_{s+}|\cos(\omega_1 t + \theta_{i+}), \\ i_{s\beta+} = |\boldsymbol{I}_{s+}|\sin(\omega_1 t + \theta_{i+}) \\ i_{s\alpha-} = |\boldsymbol{I}_{s-}|\cos(-\omega_1 t + \theta_{i-}), \\ i_{s\beta-} = |\boldsymbol{I}_{s-}|\sin(-\omega_1 t + \theta_{i-}) \end{cases} \tag{4}$$

where $|\boldsymbol{U}_{s+}|$, $|\boldsymbol{U}_{s-}|$, $|\boldsymbol{I}_{s+}|$, $|\boldsymbol{I}_{s-}|$ are the amplitudes of positive and negative sequence components of the voltage and current phasors, θ_{u+}, θ_{u-}, θ_{i+}, θ_{i-} are the initial phase angles of positive and negative sequence components of the voltage and current phasors, respectively.

And the delayed stator voltages can be expressed as

$$\begin{cases} u'_{s\alpha+} = |\boldsymbol{U}_{s+}|\cos(\omega_1 t + \theta_{u+} - \pi/2) \\ \quad\quad = |\boldsymbol{U}_{s+}|\sin(\omega_1 t + \theta_{u+}) = u_{s\beta+} \\ u'_{s\beta+} = |\boldsymbol{U}_{s+}|\sin(\omega_1 t + \theta_{u+} - \pi/2) \\ \quad\quad = -|\boldsymbol{U}_{s+}|\cos(\omega_1 t + \theta_{u+}) = -u_{s\alpha+} \\ u'_{s\alpha-} = |\boldsymbol{U}_{s-}|\cos(-\omega_1 t + \theta_{u-} + \pi/2) \\ \quad\quad = -|\boldsymbol{U}_{s-}|\sin(-\omega_1 t + \theta_{u-}) = -u_{s\beta-} \\ u'_{s\beta-} = |\boldsymbol{U}_{s-}|\sin(-\omega_1 t + \theta_{u-} + \pi/2) \\ \quad\quad = |\boldsymbol{U}_{s-}|\cos(-\omega_1 t + \theta_{u-}) = u_{s\alpha-} \end{cases}. \tag{5}$$

It can be seen from (1), (2), and (5) that the extended active power is the same as the traditional one when there are only positive voltage components, which means when the extended active power is applied, the control strategy can still work well under balanced gird condition.

The extended active power, traditional reactive power and electromagnetic torque under unbalanced grid condition are complicated and have oscillating components, which can be expressed as

$$\begin{cases} P_s^{\text{new}} = P_{s0}^{\text{new}} + P_{si2}^{\text{new}} + P_{su2}^{\text{new}} \\ Q_s = Q_{s0} + Q_{si2} + Q_{su2} \\ T_s = T_{s0} + T_{si2} + T_{su2} \end{cases} \tag{6}$$

where P_{s0}^{new}, Q_{s0}, and T_{e0} are the average components of the extended active power, traditional reactive power, and electromagnetic torque, respectively; $P_{\text{si2}}^{\text{new}}$, Q_{si2}, and T_{ei2} are the oscillating components at twice the grid frequency caused by negative sequence current and positive sequence voltage; $P_{\text{su2}}^{\text{new}}$, Q_{su2}, and T_{eu2} are the oscillating components at twice the grid frequency caused by negative sequence voltage and positive sequence current, respectively.

For a clear illustration, the values of the power ripples can be represented as follows:

$$\begin{cases} P_{si2}^{\text{new}} = \dfrac{3}{2}\left(u'_{s\alpha+} i_{s\beta-} - u'_{s\beta+} i_{s\alpha-}\right) \\ \quad\quad = \dfrac{3}{2}\left(u_{s\beta+} i_{s\beta-} + u_{s\alpha+} i_{s\alpha-}\right) \\ \quad\quad = \dfrac{3}{2}|U_{s+}||I_{s-}|\cos(2\omega_1 t + \theta_{u+} - \theta_{i-}) \\ P_{su2}^{\text{new}} = \dfrac{3}{2}\left(u'_{s\alpha-} i_{s\beta+} - u'_{s\beta-} i_{s\alpha+}\right) \\ \quad\quad = -\dfrac{3}{2}\left(u_{s\beta-} i_{s\beta+} + u_{s\alpha-} i_{s\alpha+}\right) \\ \quad\quad = -\dfrac{3}{2}|U_{s-}||I_{s+}|\cos(2\omega_1 t + \theta_{i+} - \theta_{u-}) \end{cases} \tag{7}$$

$$\begin{cases} Q_{si2} = \dfrac{3}{2}\left(u_{s\beta+} i_{s\alpha-} - u_{s\alpha+} i_{s\beta-}\right) \\ \quad\quad = \dfrac{3}{2}|U_{s+}||I_{s-}|\sin(2\omega_1 t + \theta_{u+} - \theta_{i-}) \\ Q_{su2} = \dfrac{3}{2}\left(u_{s\beta-} i_{s\alpha+} - u_{s\alpha-} i_{s\beta+}\right) \\ \quad\quad = -\dfrac{3}{2}|U_{s-}||I_{s+}|\sin(2\omega_1 t + \theta_{i+} - \theta_{u-}) \end{cases}. \tag{8}$$

Ignoring the influence of stator resistance, the ripples of electromagnetic torque can be expressed as follows:

$$\begin{cases} T_{ei2} = \dfrac{3}{2\omega_1}\left(u_{s\alpha+} i_{s\alpha-} + u_{s\beta+} i_{s\beta-}\right) \\ \quad\quad = \dfrac{3}{2\omega_1}|U_{s+}||I_{s-}|\cos(2\omega_1 t + \theta_{u+} - \theta_{i-}) \\ T_{eu2} = -\dfrac{3}{2\omega_1}\left(u_{s\alpha-} i_{s\alpha+} + u_{s\beta-} i_{s\beta+}\right) \\ \quad\quad = -\dfrac{3}{2\omega_1}|U_{s-}||I_{s+}|\cos(2\omega_1 t + \theta_{i+} - \theta_{u-}) \end{cases}. \tag{9}$$

It can be concluded from (7) and (9) that

$$\begin{cases} T_{ei2} = \dfrac{P_{si2}^{\text{new}}}{\omega_1} \\ T_{eu2} = \dfrac{P_{su2}^{\text{new}}}{\omega_1} \end{cases}. \tag{10}$$

According to (10), the ripples of the extended active power and electromagnetic torque can be eliminated at the same time. Therefore, the control objective of the extended active power can be set as follows:

$$P_{si2}^{\text{new}} + P_{su2}^{\text{new}} = 0 \tag{11}$$

According to (7) and (11), equations (12) can be obtained as

$$\begin{cases} |U_{s+}||I_{s-}| = |U_{s-}||I_{s+}| \\ \cos(2\omega_1 t + \theta_{u+} - \theta_{i-}) = \cos(2\omega_1 t + \theta_{i+} - \theta_{u-}) \end{cases} \tag{12}$$

Thus, the initial phase angles of the voltage and current phasors will meet the following equation:

$$\theta_{u+} - \theta_{i-} = \theta_{i+} - \theta_{u-} \tag{13}$$

It can be seen from (8), (12) and (13) that the reactive power ripples will also be eliminated under this condition. Therefore,

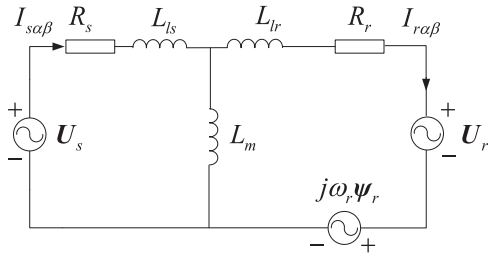

Fig. 2. Equivalent circuit of DFIG in stationary reference frame.

equations (14) can be set as the control target to eliminate the power ripples and electromagnetic torque ripples

$$\begin{cases} P_{si2}^{\text{new}} + P_{su2}^{\text{new}} = 0 \\ Q_{si2} + Q_{su2} = 0 \end{cases}. \tag{14}$$

The flux of DFIG in stationary $\alpha\beta$ reference frame can be expressed as

$$\begin{cases} \boldsymbol{\psi}_{s\alpha\beta} = L_s \boldsymbol{I}_{s\alpha\beta} + L_m \boldsymbol{I}_{r\alpha\beta} \\ \boldsymbol{\psi}_{r\alpha\beta} = L_r \boldsymbol{I}_{r\alpha\beta} + L_m \boldsymbol{I}_{s\alpha\beta} \end{cases}. \tag{15}$$

Equation (15) can be transformed as

$$\begin{cases} \boldsymbol{\psi}_{s\alpha\beta} = L_m \left(1 - \dfrac{L_r L_s}{L_m^2}\right) \boldsymbol{I}_{r\alpha\beta} + \dfrac{L_s}{L_m} \boldsymbol{\psi}_{r\alpha\beta} \\ \boldsymbol{\psi}_{r\alpha\beta} = L_m \left(1 - \dfrac{L_r L_s}{L_m^2}\right) \boldsymbol{I}_{s\alpha\beta} + \dfrac{L_r}{L_m} \boldsymbol{\psi}_{s\alpha\beta} \end{cases}. \tag{16}$$

We can set

$$\sigma' = (L_r L_s / L_m^2 - 1) = \sigma L_r L_s / L_m^2 \tag{17}$$

where σ is the magnetic leakage factor, i.e.

$$\sigma = 1 - L_m^2 / L_s L_r. \tag{18}$$

According to (16) and (17), the following can be obtained:

$$\begin{cases} \boldsymbol{\psi}_{s\alpha\beta} = -\sigma' L_m \boldsymbol{I}_{r\alpha\beta} + \dfrac{L_s}{L_m} \boldsymbol{\psi}_{r\alpha\beta} \\ \boldsymbol{\psi}_{r\alpha\beta} = -\sigma' L_m \boldsymbol{I}_{s\alpha\beta} + \dfrac{L_r}{L_m} \boldsymbol{\psi}_{s\alpha\beta} \end{cases}. \tag{19}$$

And the stator and rotor voltages can be expressed as

$$\begin{cases} \boldsymbol{U}_{s\alpha\beta} = R_s \boldsymbol{I}_{s\alpha\beta} + \dfrac{d\boldsymbol{\psi}_{s\alpha\beta}}{dt} \\ \boldsymbol{U}_{r\alpha\beta} = R_r \boldsymbol{I}_{r\alpha\beta} + \dfrac{d\boldsymbol{\psi}_{r\alpha\beta}}{dt} - j\omega_r \boldsymbol{\psi}_{r\alpha\beta} \end{cases}. \tag{20}$$

The equivalent circuit of DFIG in stationary reference frame is shown in Fig. 2.

According to (2), the derivative of power can be expressed as

$$\begin{cases} \dfrac{dP_s^{\text{new}}}{dt} = -\dfrac{3}{2}\text{Im}\left(\dfrac{d\boldsymbol{I}_{s\alpha\beta}^*}{dt}\boldsymbol{U}'_{s\alpha\beta} + \boldsymbol{I}_{s\alpha\beta}^* \dfrac{d\boldsymbol{U}'_{s\alpha\beta}}{dt}\right) \\ \dfrac{dQ_s}{dt} = \dfrac{3}{2}\text{Im}\left(\dfrac{d\boldsymbol{I}_{s\alpha\beta}^*}{dt}\boldsymbol{U}_{s\alpha\beta} + \boldsymbol{I}_{s\alpha\beta}^* \dfrac{d\boldsymbol{U}_{s\alpha\beta}}{dt}\right) \end{cases}. \tag{21}$$

Substituting (15) into (20) and ignoring the influence of stator and rotor resistance, the derivative of stator current can be calculated as

$$\frac{d\boldsymbol{I}_{s\alpha\beta}}{dt} = -\frac{1}{\sigma' L_m} \times \left[\boldsymbol{U}_{r\alpha\beta} - \frac{L_r}{L_m}\boldsymbol{U}_{s\alpha\beta} + j\omega_r\left(-\sigma' L_m \boldsymbol{I}_{s\alpha\beta} + \frac{L_r}{L_m}\boldsymbol{\psi}_{s\alpha\beta}\right)\right]. \tag{22}$$

The original and delayed stator voltages under unbalanced grid condition can be expressed as

$$\begin{aligned} \mathbf{U}_{s\alpha\beta} &= \mathbf{U}_{s\alpha\beta+} + \mathbf{U}_{s\alpha\beta-} \\ &= |\boldsymbol{U}_{s+}| e^{j(\omega_1 t + \theta_{u+})} + |\boldsymbol{U}_{s-}| e^{-j(\omega_1 t + \theta_{u-})} \end{aligned} \tag{23}$$

$$\begin{aligned} \mathbf{U}'_{s\alpha\beta} &= \mathbf{U}'_{s\alpha\beta+} + \mathbf{U}'_{s\alpha\beta-} \\ &= |\boldsymbol{U}_{s+}| e^{j(\omega_1 t + \theta_{u+} - \pi/2)} + |\boldsymbol{U}_{s-}| e^{j(-\omega_1 t + \theta_{u-} + \pi/2)} \\ &= -j|\boldsymbol{U}_{s+}| e^{j(\omega_1 t + \theta_{u+})} + j|\boldsymbol{U}_{s-}| e^{j(-\omega_1 t + \theta_{u-})} \\ &= -j\mathbf{U}_{s\alpha\beta+} + j\mathbf{U}_{s\alpha\beta-}. \end{aligned} \tag{24}$$

In stationary reference frame, the derivative of stator voltage can be expressed as

$$\begin{aligned} \frac{d\boldsymbol{U}_{s\alpha\beta}}{dt} &= j\omega_1 |\boldsymbol{U}_{s+}| e^{j(\omega_1 t + \theta_{u+})} - j\omega_1 |\boldsymbol{U}_{s-}| e^{j(-\omega_1 t + \theta_{u-})} \\ &= j\omega_1 \boldsymbol{U}_{s\alpha\beta+} - j\omega_1 \boldsymbol{U}_{s\alpha\beta-} = -\omega_1 \boldsymbol{U}'_{s\alpha\beta} \end{aligned} \tag{25}$$

$$\begin{aligned} \frac{d\boldsymbol{U}'_{s\alpha\beta}}{dt} &= (-j) j\omega_1 \boldsymbol{U}_{s\alpha\beta+} + j(-j\omega_1 \boldsymbol{U}_{s\alpha\beta-}) \\ &= \omega_1 \boldsymbol{U}_{s\alpha\beta+} + \omega_1 \boldsymbol{U}_{s\alpha\beta-} = \omega_1 \boldsymbol{U}_{s\alpha\beta}. \end{aligned} \tag{26}$$

Substituting (22), (25), and (26) into (21), the derivative of power can be obtained as

$$\begin{cases} \dfrac{dP_s^{\text{new}}}{dt} = -\dfrac{3L_r}{2\sigma' L_m^2}\text{Im}(\boldsymbol{U}_{s\alpha\beta}^* \boldsymbol{U}'_{s\alpha\beta}) + \dfrac{3}{2\sigma' L_m}\text{Im}(\boldsymbol{U}_{r\alpha\beta}^* \boldsymbol{U}'_{s\alpha\beta}) \\ \quad + \dfrac{3L_r\omega_r}{2\sigma' L_m^2}\text{Im}(\boldsymbol{\psi}_{s\alpha\beta}^* \boldsymbol{U}'_{s\alpha\beta}) - \dfrac{3\omega_r}{2}\text{Re}(\boldsymbol{I}_{s\alpha\beta}^* \boldsymbol{U}'_{s\alpha\beta}) - \omega_1 Q_s \\ \dfrac{dQ_s}{dt} = -\dfrac{3}{2\sigma' L_m}\text{Im}(\boldsymbol{U}_{r\alpha\beta}^* \boldsymbol{U}_{s\alpha\beta}) - \dfrac{3L_r\omega_r}{2\sigma' L_m^2}\text{Im}(\boldsymbol{\psi}_{s\alpha\beta}^* \boldsymbol{U}_{s\alpha\beta}) \\ \quad + \omega_r P_s + \omega_1 P_s^{\text{new}} \end{cases}. \tag{27}$$

It can also be expressed in the matrix form, i.e.

$$\begin{aligned} \frac{d}{dt}\begin{bmatrix} P_s^{\text{new}} \\ Q_s \end{bmatrix} = &-\frac{3}{2\sigma' L_m}\begin{bmatrix} -u'_{s\beta} & u'_{s\alpha} \\ u_{s\beta} & -u_{s\alpha} \end{bmatrix}\begin{bmatrix} u_{r\alpha} \\ u_{r\beta} \end{bmatrix} \\ &+ \frac{3L_r}{2\sigma' L_m^2}\begin{bmatrix} u_{s\beta}u'_{s\alpha} - u_{s\alpha}u'_{s\beta} \\ 0 \end{bmatrix} \\ &- \frac{3L_r\omega_r}{2\sigma' L_m^2}\begin{bmatrix} \psi_{s\beta}u'_{s\alpha} - \psi_{s\alpha}u'_{s\beta} \\ \psi_{s\alpha}u_{s\beta} - \psi_{s\beta}u_{s\alpha} \end{bmatrix} \\ &+ \begin{bmatrix} -\omega_1 Q_s - 3/2\omega_r(u'_{s\alpha}i_{s\alpha} + u'_{s\beta}i_{s\beta}) \\ \omega_1 P_s^{\text{new}} + 3/2\omega_r(u_{s\alpha}i_{s\alpha} + u_{s\beta}i_{s\beta}) \end{bmatrix}. \end{aligned} \tag{28}$$

III. SMDPC for DFIG Using Extended Active Power

The control target for the proposed SMDPC system is to make the extended active power and traditional reactive power follow their reference values. In order to minimize the steady-state error and retain the good dynamic performance, the integral form sliding surface can be selected [8]. Thus, the sliding surface is set as

$$\boldsymbol{S} = \begin{bmatrix} S_1 & S_2 \end{bmatrix}^T \tag{29}$$

$$\begin{cases} S_1 = e_p + K_p \int_0^t e_p(\tau)d\tau \\ S_2 = e_q + K_q \int_0^t e_q(\tau)d\tau \end{cases} \tag{30}$$

where K_p and K_q are the integral parameters of the extended active power and traditional reactive power, respectively. e_p and e_q are the tracking errors of the extended active power and traditional reactive power, respectively, i.e.

$$\begin{cases} e_p = P_{\text{sref}}^{\text{new}} - P_s^{\text{new}} \\ e_q = Q_{\text{sref}} - Q_s \end{cases}. \tag{31}$$

In order to drive the state orbit to the sliding surface, a Lyapunov function is defined as

$$W = \frac{1}{2}\boldsymbol{S}^T\boldsymbol{S} = \frac{1}{2}(S_1^2 + S_2^2) \geq 0. \tag{32}$$

The derivative of *W* can be calculated as

$$\frac{dW}{dt} = = S_1\frac{dS_1}{dt} + S_2\frac{dS_2}{dt} = \boldsymbol{S}^T\frac{d\boldsymbol{S}}{dt}. \tag{33}$$

According to (30) and (31), the following can be obtained:

$$\frac{d\boldsymbol{S}}{dt} = \frac{d}{dt}\begin{bmatrix} S_1 \\ S_2 \end{bmatrix} = -\frac{d}{dt}\begin{bmatrix} P_s^{\text{new}} \\ Q_s \end{bmatrix} + \begin{bmatrix} K_p e_p \\ K_q e_q \end{bmatrix} \tag{34}$$

Taking (28) into (34), the following equation can be calculated:

$$\frac{d\boldsymbol{S}}{dt} = \boldsymbol{G} + \boldsymbol{DU} \tag{35}$$

where

$$\begin{aligned} \boldsymbol{G} = & -\frac{3L_r}{2\sigma' L_m^2}\begin{bmatrix} u_{s\beta}u'_{s\alpha} - u_{s\alpha}u'_{s\beta} \\ 0 \end{bmatrix} \\ & + \frac{3L_r\omega_r}{2\sigma' L_m^2}\begin{bmatrix} \psi_{s\beta}u'_{s\alpha} - \psi_{s\alpha}u'_{s\beta} \\ \psi_{s\alpha}u_{s\beta} - \psi_{s\beta}u_{s\alpha} \end{bmatrix} \\ & - \begin{bmatrix} -\omega_1 Q_s - 3/2\omega_r(u'_{s\alpha}i_{s\alpha} + u'_{s\beta}i_{s\beta}) \\ \omega_1 P_s^{\text{new}} + 3/2\omega_r(u_{s\alpha}i_{s\alpha} + u_{s\beta}i_{s\beta}) \end{bmatrix} + \begin{bmatrix} K_p e_p \\ K_q e_q \end{bmatrix} \end{aligned}$$

$$\boldsymbol{D} = \frac{3}{2\sigma' L_m}\begin{bmatrix} -u'_{s\beta} & u'_{s\alpha} \\ u_{s\beta} & -u_{s\alpha} \end{bmatrix} \qquad \boldsymbol{U} = \begin{bmatrix} u_{r\alpha} \\ u_{r\beta} \end{bmatrix}$$

According to (33) and (35), the following can be obtained:

$$\frac{dW}{dt} = \boldsymbol{S}^T(\boldsymbol{G} + \boldsymbol{DU}). \tag{36}$$

For the purpose of $dW/dt \leq 0$, the switching control law can be designed as follows:

$$\boldsymbol{U} = -\boldsymbol{D}^{-1}\left\{\boldsymbol{G} + \begin{bmatrix} K_{ps} & 0 \\ 0 & K_{qs} \end{bmatrix}\begin{bmatrix} \text{sgn}(S_1) \\ \text{sgn}(S_2) \end{bmatrix}\right\} \tag{37}$$

where K_{ps} and K_{qs} are the parameters of switching control laws for the extended active power and traditional reactive power, respectively. $\text{sgn}(S_1)$ and $\text{sgn}(S_2)$ are the switching functions for the extended active power and traditional reactive power, respectively.

Therefore

$$\frac{dW}{dt} = -\begin{bmatrix} S_1 & S_2 \end{bmatrix}\begin{bmatrix} K_{ps} & 0 \\ 0 & K_{qs} \end{bmatrix}\begin{bmatrix} \text{sgn}(S_1) \\ \text{sgn}(S_2) \end{bmatrix} \leq 0. \tag{38}$$

It can be seen that *W* is a positive-definite function and the derivative of *W* is a negative-definite function, which implies that S_1 and S_2 go to zero asymptotically. According to Lyapunov stability theorem, the stability of the proposed SMDPC strategy can be guaranteed.

The robustness of the proposed SMDPC can be proved as follow. In the practical application, the control performance of the DFIG system will be affected by the parameter variation, external disturbance and so on. The disturbance mentioned earlier can be represented as $\boldsymbol{N}$, i.e.

$$\boldsymbol{N} = \begin{bmatrix} N_1 & N_2 \end{bmatrix}^T \tag{39}$$

where N_1 and N_2 represent the influence to the extended active power and traditional reactive power, respectively.

Thus, the following equation can be obtained:

$$\frac{d\boldsymbol{S}}{dt} = \boldsymbol{G} + \boldsymbol{DU} + \boldsymbol{N}. \tag{40}$$

Taking (37) and (40) into (33), the derivative of *W* can be rewritten as

$$\frac{dW}{dt} = -\begin{bmatrix} S_1 & S_2 \end{bmatrix}\begin{bmatrix} K_{ps}\text{sgn}(S_1) - N_1 \\ K_{qs}\text{sgn}(S_2) - N_2 \end{bmatrix}. \tag{41}$$

If K_{ps} and K_{qs} are big enough to fulfill (42), the derivative of *W* can be guaranteed as a negative value. According to Lyapunov stability theorem, the robustness of the proposed SMDPC is pretty good when the parameters are selected properly

$$\begin{cases} K_{ps} \geq |N_1| \\ K_{qs} \geq |N_2| \end{cases}. \tag{42}$$

As the traditional switching control law would introduce the chattering problem into the control system, a boundary layer around the sliding surface proposed in [8] is adopted in this paper to solve the problem, where the switching functions can be rewritten as

$$\text{sgn}(S_j) = \begin{cases} 1, & S_j > \lambda_j \\ \frac{S_j}{\lambda_j}, & |S_j| \leq \lambda_j \\ -1, & S_j < -\lambda_j \end{cases} \tag{43}$$

where λ_j is the width of the boundary layer and $j = 1, 2$.

The control block diagram of the proposed SMDPC strategy for DFIG is shown in Fig. 3. First, the measured stator voltage $\boldsymbol{U}_{\text{sabc}}$ and current $\boldsymbol{I}_{\text{sabc}}$ are transformed into $\boldsymbol{U}_{s\alpha\beta}$, and $\boldsymbol{I}_{s\alpha\beta}$, and the $\boldsymbol{U}_{s\alpha\beta}$ is lagged by a quarter of the fundamental period to obtain $\boldsymbol{U}'_{s\alpha\beta}$. Then, the stator flux is estimated using stator voltage, and the extended active power and traditional reactive power are calculated according to (1) and (2). In addition, the

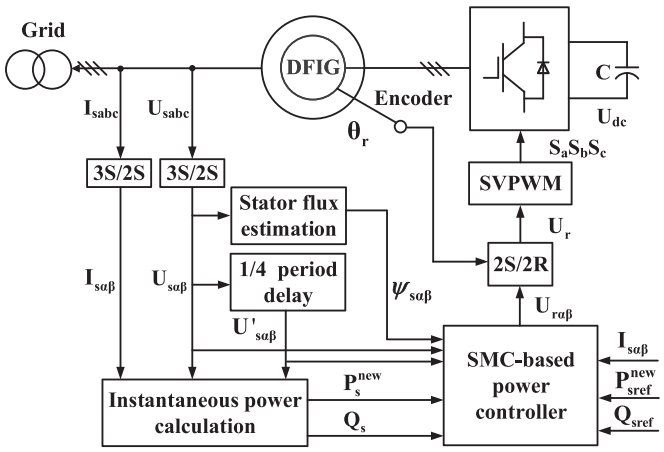

Fig. 3. Control block diagram of the proposed SMDPC for DFIG.

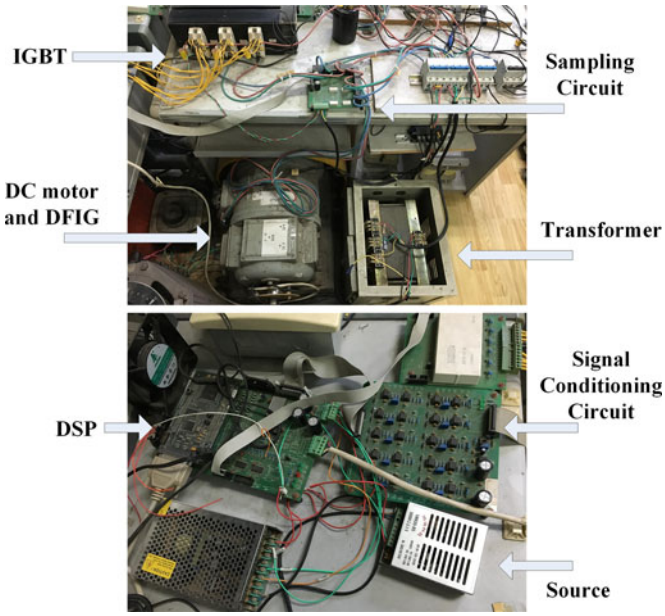

Fig. 4. Experimental platform.

reference value and the real value of powers as well as stator voltage, flux and current are used as the input of the SMC-based power controller. Thus, the reference rotor voltage can be deduced and transformed into rotor reference frame. Finally, the switching signal is produced according to U_r using SVPWM unit. It can be seen the control system is very simple and there is no need of decomposition process of positive and negative sequence components and PLL block in the proposed strategy.

IV. Experimental Studies

A. Experimental Setup

Experimental studies are conducted to validate the effectiveness of the SMDPC strategy using the proposed extended active power. The experimental platform is set up as shown in Fig. 4. The wind turbine is emulated by a dc motor, and a TMS320F2812 DSP is employed as the microprocessor. The unbalanced grid voltage is emulated by making one phase of the voltage drop to 50% using a transformer. The dc-bus voltage is assumed to be controlled as a constant value by the grid-side converter, since we concentrate on the control strategy of the DFIG in this paper. Parameters of the DFIG system are listed in Table I.

TABLE I
Parameters of DFIG

System Parameters	Value
Grid voltage	220 V (line voltage)
Rated power	2000 W
Rated frequency	50 Hz
Poles	4
Stator resistance	1.9188 Ω
Stator leakage inductance	0.00744 H
Rotor resistance	2.5712 Ω
Rotor leakage inductance	0.00744 H
Mutual inductance	0.234 H
Stator/rotor turns ratio	1.9485
DC-bus voltage	120 V

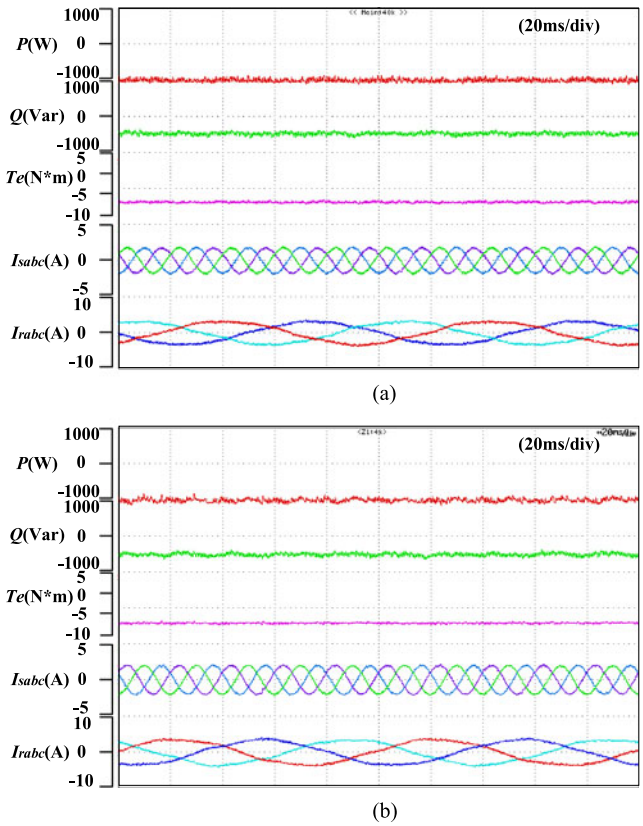

Fig. 5. Steady-state performance of different control strategies under balanced grid condition. (a) Traditional SMDPC. (b) Novel SMDPC.

Comparative experimental studies are conducted for the SMDPC using the extended and traditional active powers under both balanced and unbalanced grid conditions. The sampling frequency and switching frequency are both set to 10 kHz. All the experimental results are shown in Figs. 5–14. The rotor is running at 40 Hz in all the experimental studies. In order to simplify the analysis, we use novel SMDPC to denote SMDPC using the extended active power and traditional SMDPC to designate SMDPC using the traditional active power in the following sections.

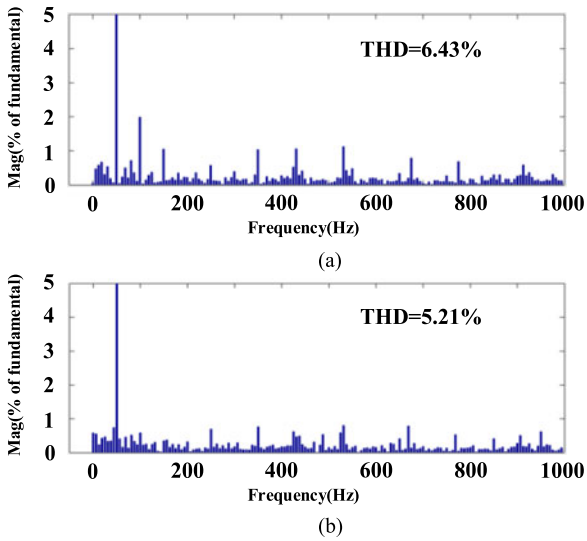

Fig. 6. Harmonic spectrum analyses of stator current for different control strategies under balanced grid condition. (a) Traditional SMDPC. (b) Novel SMDPC.

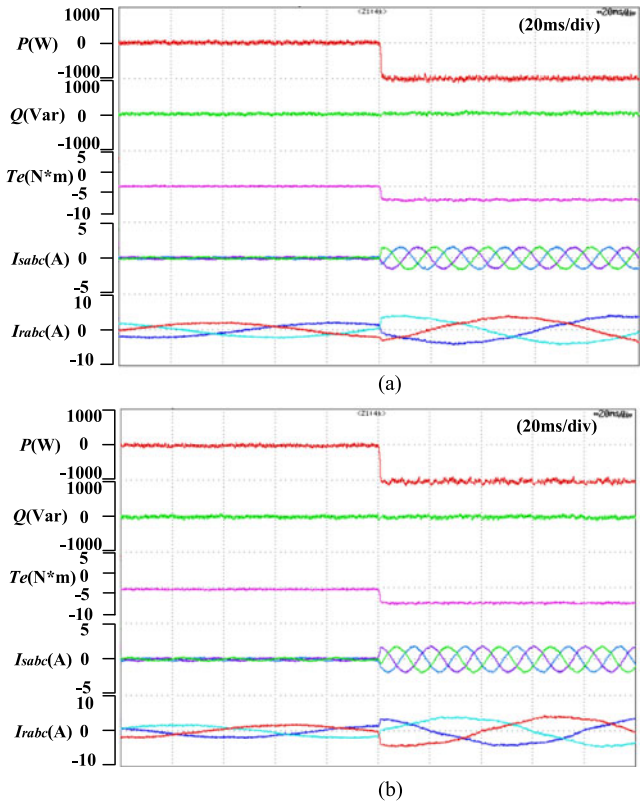

Fig. 7. Power step response of different control strategies under balanced grid condition. (a) Traditional SMDPC. (b) Novel SMDPC.

B. Experimental Results

Fig. 5 shows the steady-state performance of the traditional and novel SMDPCs when the DFIG sends 1000 W active power and 500 Var reactive power to the power grid under balanced grid condition. The total harmonic distortion (THD) analyses of stator current for different control strategies are shown in Fig. 6. It can be observed that the steady-state performances of the two control strategies are similar. And the

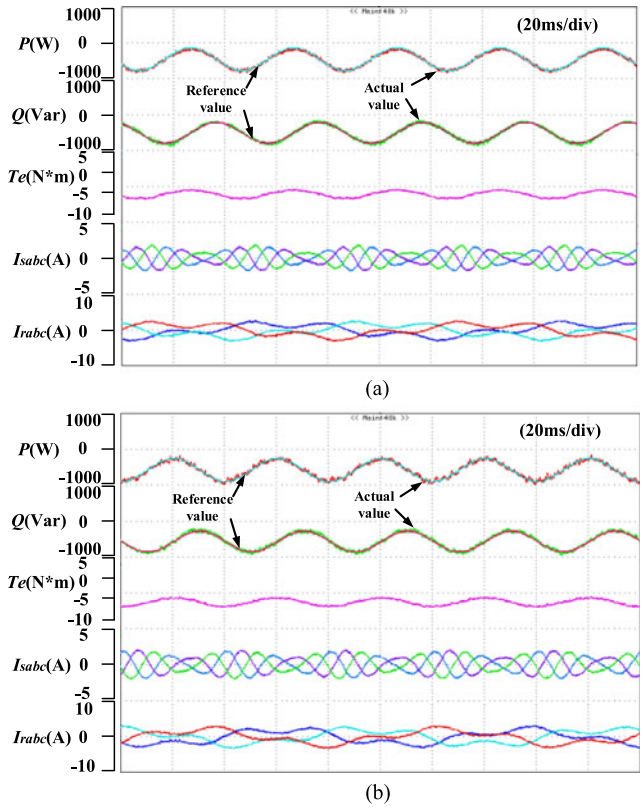

Fig. 8. Control performance of different control strategies when varying reference of power is given under balanced grid condition. (a) Traditional SMDPC. (b) Novel SMDPC.

stator current THD of the novel SMDPC is 5.21%, a little lower than 6.43% of the traditional one. This is because the grid voltage is produced by the transformer in our lab, which is not ideal. There are still some harmonics, which will influence the stator currents. As analyzed in Section II, the novel SMDPC can restrain the current harmonics while the traditional one cannot. Therefore, the novel SMDPC can achieve a better current control performance than the traditional one under this condition.

Fig. 7 compares the dynamic power step responses of the traditional and novel SMDPCs under balanced grid condition. The active power reference changes from 0 to −1000 W, and the reactive power is controlled to be 0 Var. It can be seen that the step response time is very short, which means the dynamic performance of both control strategies are pretty good.

Fig. 8 shows the control performances of the traditional and novel SMDPCs when a sine variation of the power reference is given under balanced grid condition. The reference active and reactive powers are shown in blue and red, respectively. And the actual active and reactive powers are shown in red and green, respectively. It can be seen when the power reference changes, both strategies can follow the reference power very well, which proves the transient performances of the two strategies are also satisfying.

Steady-state performance for the traditional and novel SMDPCs under unbalanced grid condition is shown in Fig. 9. The DFIG sends 1000 W active power and 500 Var reactive power to the power grid. The harmonic spectrum analyses of stator

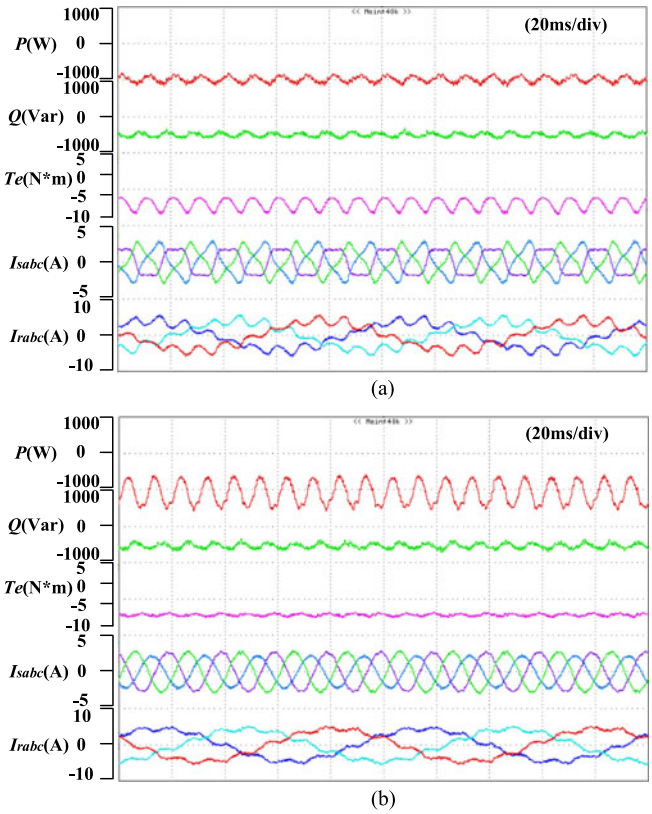

Fig. 9. Steady-state performance of different control strategies under unbalanced grid condition. (a) Traditional SMDPC. (b) Novel SMDPC.

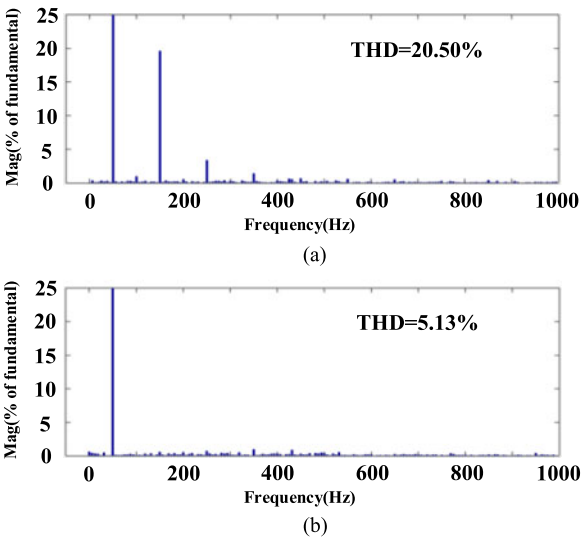

Fig. 10. Harmonic spectrum analyses of stator current for different control strategies under unbalanced grid condition. (a) Traditional SMDPC. (b) Novel SMDPC.

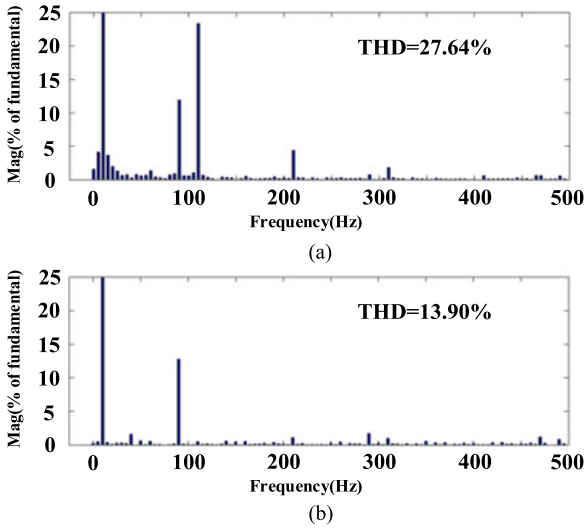

Fig. 11. Harmonic spectrum analyses of rotor current for different control strategies under unbalanced grid condition. (a) Traditional SMDPC. (b) Novel SMDPC.

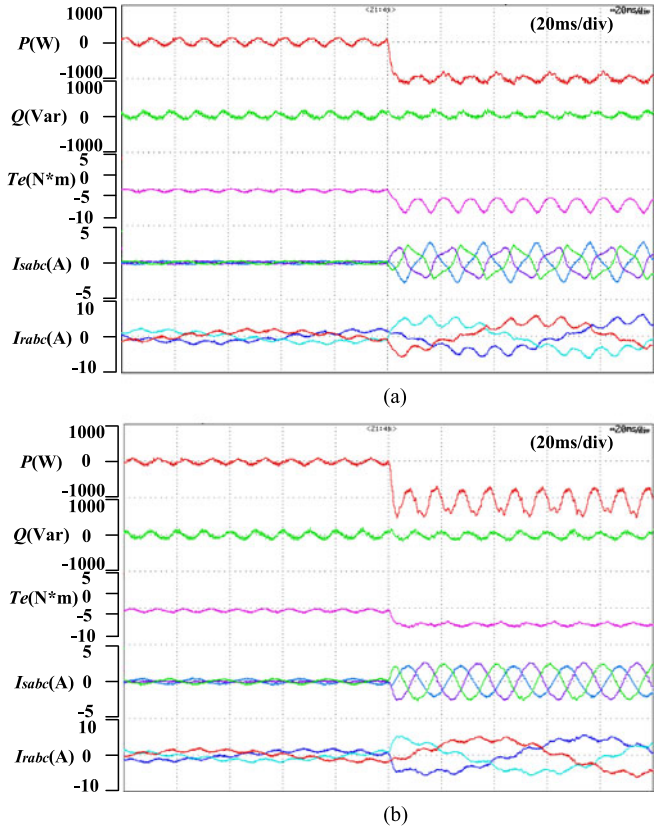

Fig. 12. Power step response of different control strategies under unbalanced grid condition. (a) Traditional SMDPC. (b) Novel SMDPC.

and rotor currents are shown in Figs. 10 and 11, respectively. It can be seen when the traditional SMDPC is applied to DFIG, the electromagnetic torque contains ripples at twice the grid frequency, and the stator current contains a lot of third sequence harmonic components. The fundamental frequency of rotor current is 10 Hz because the rotor is running at 40 Hz. There are 11th (110 Hz) and 9th (−90 Hz) sequence harmonic components in rotor currents. Thus, it can be deduced that there are third sequence harmonic components (150 Hz) and negative sequence harmonic components (−50 Hz) in stator currents, which coincides with the analysis in Section II.

As for the novel SMDPC, the electromagnetic torque ripples are effectively restrained and the current is sinusoidal. The stator

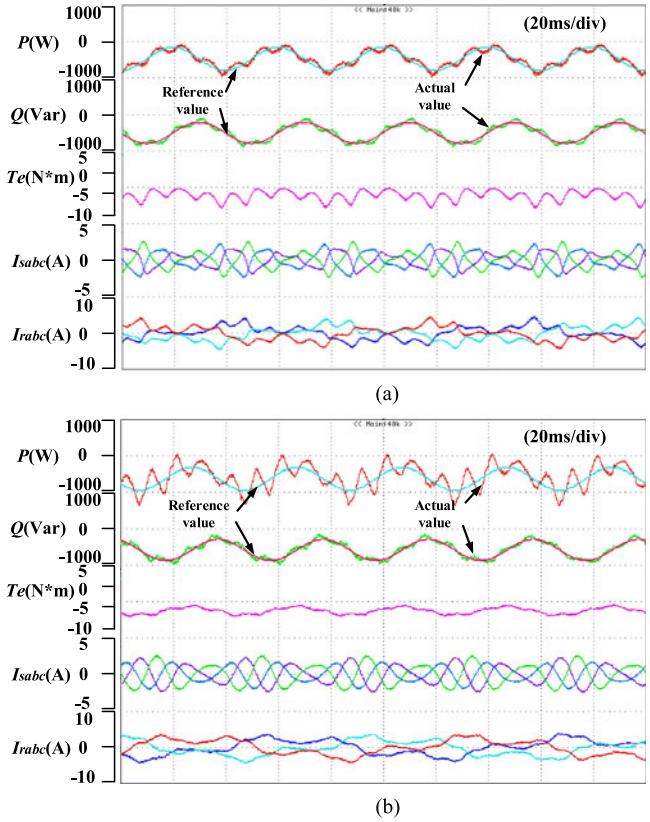

Fig. 13. Control performance of different control strategies when varying reference of power is given under unbalanced grid condition. (a) Traditional SMDPC. (b) Novel SMDPC.

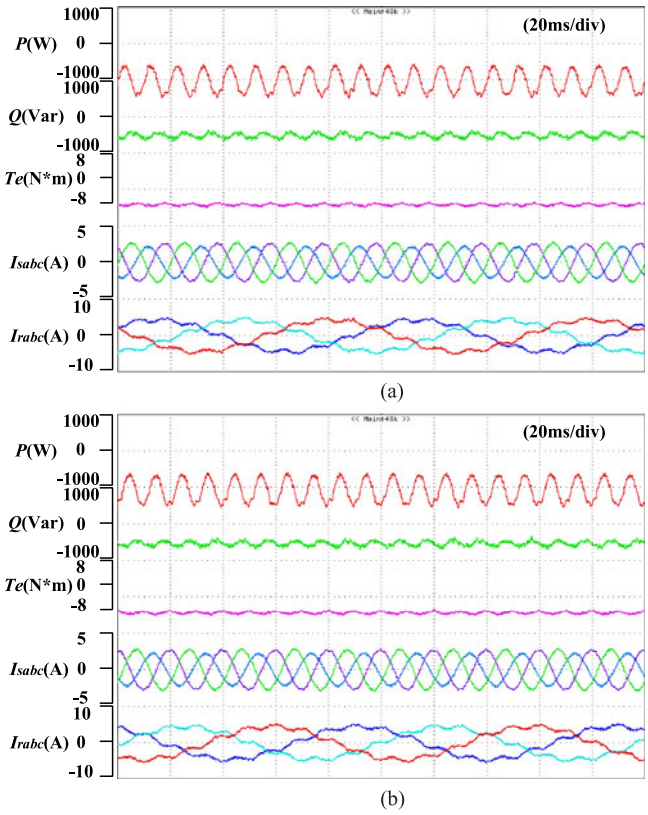

Fig. 14. Steady-state performance of the novel SMDPC when parameter L_{m} varies. (a) $L_{\mathrm{m}}{}' = 2L_{\mathrm{m}}$. (b) $L_{\mathrm{m}}{}' = 0.5L_{\mathrm{m}}$.

current harmonics are much lower and the third sequence harmonic current components are restrained effectively. Thus, the 11th sequence harmonic components are also restrained in rotor currents. It can be observed that there are still 9th sequence harmonic components in rotor currents, which means the negative sequence components still exist in stator currents. The active power contains ripples because the extended active power is selected as the control target to obtain sinusoidal stator currents.

Fig. 12 shows the dynamic power step responses for the traditional and novel SMDPCs under unbalanced gird condition. The power reference is the same as Fig. 7. It can be seen that the step response time is still very short, which means the dynamic performance of the two control strategies are still good under unbalanced gird condition. In addition, the stator current is still sinusoidal when the power step occurs for the novel SMDPC.

Fig. 13 shows the control performances of the two strategies when a sine variation of the power reference is given under unbalanced grid condition. It can be seen that the stator currents, reactive power and electromagnetic torque of the novel SMDPC are still similar as that in Fig. 8(b). Although the active power contains ripples because the extended active power is selected as the control target, its average value still follows the reference power. Therefore, we can conclude that the novel SMDPC can still restrain the stator current harmonics and electromagnetic torque ripples when the power reference is changing, and its transient performance is still satisfying. As for the traditional SMDPC, it can follow the reference power better under unbalanced grid condition. However, the electromagnetic torque contains large ripples and the stator currents are distorted compared with Fig. 8(a), which is very harmful to the power gird and the wind turbine.

The robustness of the novel SMDPC is experimentally validated in Fig. 14 by varying the mutual inductance L_{m}. In Fig. 14(a), the mutual inductance value is set to 0.468 H in the program, which is twice of the actual mutual inductance. In Fig. 14(b), its value is set to 0.117 H, which is only half of the actual mutual inductance. It can be seen from the experimental results that the control performance under those conditions is nearly the same as Fig 9(b), which means that the robustness of the proposed control strategy is pretty good.

V. Conclusion

An SMDPC strategy for DFIG using extended active power has been proposed in this paper under both balanced and unbalanced grid conditions. Comparative experimental studies based on the SMDPC using the extended and traditional active powers have been conducted to validate the effectiveness of the proposed SMDPC. The results indicate that the proposed SMDPC can achieve similar control performance as the traditional one under balanced grid condition, and it can obtain sinusoidal stator currents and restrain electromagnetic torque ripples under unbalanced grid condition without the need of decomposition process and PLL block. The experimental results also verify

that the dynamic performance of the proposed strategy is satisfactory. In addition, the robustness of the control system is validated by experimental results under unbalanced grid condition. Therefore, it can be concluded that the proposed SMDPC strategy can work well under both balanced and unbalanced grid conditions with a simple control system and reduced computational burdens.

REFERENCES

[1] Z. Chen, J. M. Guerrero, and F. Blaabjerg, "A review of the state of the art of power electronics for wind turbines," *IEEE Trans. Power Electron.*, vol. 24, no. 8, pp. 1859–1875, Aug. 2009.

[2] Y. Zhang, J. Hu, and J. Zhu, "Three-vectors-based predictive direct power control of the doubly fed induction generator for wind energy applications," *IEEE Trans. Power Electron.*, vol. 29, no. 7, pp. 3485–3500, Jul. 2014.

[3] A. Tapia, G. Tapia, J. X. Ostolaza, and J. R. Saenz, "Modeling and control of a wind turbine driven doubly fed induction generator," *IEEE Trans. Energy Convers.*, vol. 18, no. 2, pp. 194–204, Jun. 2003.

[4] H. Akagi and H. Sato, "Control and performance of a doubly-fed induction machine intended for a flywheel energy storage system," *IEEE Trans. Power Electron.*, vol. 17, no 1, pp. 109–116, Jan. 2002.

[5] L. Xu and P. Cartwright, "Direct active and reactive power control of DFIG for wind energy generation," *IEEE Trans. Energy Convers.*, vol. 21, no. 3, pp. 750–758, Sep. 2006.

[6] B. Singh and N. K. S. Naidu, "Direct power control of single VSC-based DFIG without rotor position sensor," *IEEE Trans. Ind. Appl.*, vol. 50, no. 6, pp. 4152–4163, Nov./Dec. 2014.

[7] V. I. Utkin, "Sliding mode control design principles and applications to electric drives," *IEEE Trans. Ind. Electron.*, vol. 40, no. 1, pp. 23–36, Feb. 1993.

[8] J. Hu, L. Shang, Y. He, and Z. Q. Zhu, "Direct active and reactive power regulation of grid-connected DC/AC converters using sliding mode control approach," *IEEE Trans. Power Electron.*, vol. 26, no. 1, pp. 210–222, Jan. 2011.

[9] A. Hemdani, M. Dagbagi, W. M. Naouar, L. Idkhajine, I. S. Belkhodja, and E. Monmasson, "Indirect sliding mode power control for three phase grid connected power converter," *IET Power Electron*., vol. 8, no. 6, pp. 977–985, 2015.

[10] J. Hu, H. Nian, B. Hu, Y. He, and Z. Q. Zhu, "Direct active and reactive power regulation of DFIG using sliding-mode control approach," *IEEE Trans. Energy Convers.*, vol. 25, no. 4, pp. 1028–1039, Dec. 2010.

[11] M. Tsili and S. Papathanassiou, "A review of grid code technical requirements for wind farms," *IET Renew. Power Gener.*, vol. 3, no. 3, pp. 308–332, 2009.

[12] L. Xu and Y. Wang, "Dynamic modeling and control of DFIG-based wind turbines under unbalanced network conditions," *IEEE Trans. Power Syst.*, vol. 22, no. 1, pp. 314–323, Feb. 2007.

[13] M. Castilla, J. Miret, J. Matas, A. Borrell, and L. G. de Vicuna, "Direct rotor current-mode control improves the transient response of doubly fed induction generator-based wind turbines," *IEEE Trans. Energy Convers.*, vol. 25, no. 3, pp. 722–731, Sep. 2010.

[14] J. Hu and Y. He, "Reinforced control and operation of DFIG-based wind-power-generation system under unbalanced grid voltage conditions," *IEEE Trans. Energy Convers.*, vol. 24, no. 4, pp. 905–915, Dec. 2009.

[15] J. Hu, Y. He, L. Xu, and B. W. Williams, "Improved control of DFIG systems during network unbalance using PI-R current regulators," *IEEE Trans. Ind. Electron.*, vol. 56, no. 2, pp. 439–451, Feb. 2009.

[16] J. Hu, J. Zhu, and D. G. Dorrell, "Model-predictive direct power control of doubly-fed induction generators under unbalanced grid voltage conditions in wind energy applications," *IET Renew. Power Gener.*, vol. 8, no. 6, pp. 687–695, Jan. 2014.

[17] D. Sun and X. Wang, "Low-complexity model predictive direct power control for DFIG under both balanced and unbalanced grid conditions," *IEEE Trans. Ind. Electron.*, vol. 63, no. 8, pp. 5186–5196, Aug. 2016.

[18] P. Cheng and H. Nian, "Collaborative control of DFIG system during network unbalance using reduced-order generalized integrators," *IEEE Trans. Energy Convers.*, vol. 30, no. 2, pp. 453–464, Jun. 2015.

[19] H. Nian, P. Cheng, and Z. Q. Zhu, "Coordinated direct power control of DFIG system without phase-locked loop under unbalanced grid voltage conditions," *IEEE Trans. Power Electron.*, vol. 31, no. 4, pp. 2905–2918, Apr. 2016.

[20] Y. Suh and T. A. Lipo, "Modeling and analysis of instantaneous active and reactive power for PWM AC/DC converter under generalized unbalanced network," *IEEE Trans. Power Del.*, vol. 21, no. 3, pp. 1530–1540, Jul. 2006.

[21] Y. Zhang and C. Qu, "Direct power control of a pulse width modulation rectifier using space vector modulation under unbalanced grid voltages," *IEEE Trans. Power Electron.*, vol. 30, no. 10, pp. 5892–5901, Oct. 2015.

[22] Y. Zhang and C. Qu, "Model predictive direct power control of PWM rectifiers under unbalanced network conditions," *IEEE Trans. Ind. Electron.*, vol. 62, no. 7, pp. 4011–4022, Jul. 2015.

[23] Y. Zhang and C. Qu, "Table-based direct power control for three-phase AC/DC converters under unbalanced grid voltages," *IEEE Trans. Power Electron.*, vol. 30, no. 12, pp. 7090–7099, Dec. 2015.

Dan Sun (M'05) received the B.E. degree from Shenyang Jianzhu University, Shenyang, China, in 1997, the M.S. degree from Hohai University, Nanjing, China, in 2000, and the Ph.D. degree from Zhejiang University, Hangzhou, China, in 2004, all in electrical engineering.

From 2002 to 2004, she was a joint Ph.D. student at the University of Technology, Sydney, Australia. In 2004, she joined the College of Electrical Engineering, Zhejiang University, where she has been an Associate Professor since 2008. From 2009 to 2010, she was a Visiting Scholar at the Wisconsin Electric Machines and Power Electronics Consortium, University of Wisconsin–Madison, Madison, WI, USA. Her current research interests include electric machines and drives.

Xiaohe Wang was born in 1991. He received the B.S. degree, in 2014, from Zhejiang University, Hangzhou, China, where he is currently working toward the Ph.D. degree at the College of Electrical Engineering.

His current research interests include motor control strategy in renewable-energy conversion, particularly in doubly fed induction generators for wind power generation.

Heng Nian (M'09–SM'14) received the B.Eng. degree and the M.Eng. degree from Hefei University of Technology, Hefei, China, in 1999 and 2002, respectively, and the Ph.D. degree from Zhejiang University, Hangzhou, China, in 2005, all in electrical engineering.

From 2005 to 2007, he was as a Postdoctoral with the College of Electrical Engineering, Zhejiang University. In 2007, he was promoted as an Associate Professor. Since 2016, he has been a Full Professor at the College of Electrical Engineering, Zhejiang University. From 2013 to 2014, he was a Visiting Scholar in the Department of Electrical, Computer, and System Engineering, Rensselaer Polytechnic Institute, Troy, NY, USA. His current research interests include the optimal design and operation control for wind power generation system. He has authored or coauthored more than 20 IEEE/IET Transaction papers and holds more than 20 issued/pending patents.

Z. Q. Zhu (M'90–SM'00–F'09) received the B.Eng. and M.Sc. degrees in electrical and electronic engineering from Zhejiang University, Hangzhou, China, in 1982 and 1984, respectively, and the Ph.D. degree in electronic and electrical engineering from The University of Sheffield, Sheffield, U.K., in 1991.

Since 1988, he has been with The University of Sheffield, where since 2000, he has been a Professor of Electrical Machines and Control Systems and is currently the Head of the Electrical Machines and Drives Research Group. His current research interests include design and control of permanent-magnet brushless machines and drives, for applications ranging from automotive to renewable energy.

Dr. Zhu is a Fellow of the Royal Academy of Engineering.